Available online at www.sciencedirect.com
ScienceDirect
Journal of Nuclear Materials 373 (2008) 246–253
journal of nuclear materials
www.elsevier.com/locate/jnucmat

Corrosion of ODS steels in lead–bismuth eutectic

P. Hosemann [a,b,*], H.T. Thau [c], A.L. Johnson [c], S.A. Maloy [a], N. Li [a]

[a] Los Alamos National Laboratory, P.O. Box 1663, Los Alamos, NM 87545, USA
[b] Montanuniversität Leoben, Austria
[c] University of Nevada Las Vegas, USA

Received 12 December 2006; accepted 25 May 2007

Abstract

Oxide dispersion strengthened (ODS) ferritic steels are advanced materials being developed for high temperature applications. Their properties (high temperature strength, creep resistance, corrosion/oxidation resistance) make them potentially usable for high temperature applications in liquid metal cooled systems like liquid lead–bismuth eutectic cooled reactors and spallation sources. Corrosion tests on five different ODS alloys were performed in flowing liquid lead–bismuth eutectic in the DELTA Loop at the Los Alamos National Laboratory at 535 °C for 200 h and 600 h. The tested materials were chromium alloyed ferritic/martensitic steels (12YWT, 14YWT, MA957) and Cr–Al alloyed steels (PM2000, MA956). It was shown that the Al alloyed ODS steel above 5.5 wt% Al (PM2000) is highly resistant to corrosion and oxidation in the conditions examined, and that the corrosion properties of the ODS steels depend strongly on their grain size.

1. Introduction

Liquid lead–bismuth eutectic (LBE) is a candidate material for Generation IV reactor coolant and spallation neutron targets [1]. The advantages of using LBE or lead as a nuclear coolant are derived from its physical properties such as high boiling temperature, low melting point, good thermal transport, low viscosity, low neutron capture and moderation, and high spallation neutron yield. The disadvantage of using LBE or lead is that they are aggressive media to their container and structural materials, particularly at high temperatures. To make these systems usable at high temperatures (>500 °C) new classes of materials and/or surface treatments need to be developed and tested. In a Los Alamos National Laboratory/University of Nevada Las Vegas collaboration, a liquid lead loop (lead corrosion stand, LCS) was built for testing materials at high temperatures. In support of materials selection for this loop, oxide dispersion strengthened (ODS) steels (PM2000, MA956, MA957, 12YWT and 14YWT) were tested 535 °C in LBE for 200 h and 600 h to evaluate their corrosion resistance [2–4].

2. Experiment and analysis

12YWT was produced by Kobe Steel, Ltd., Japan. 14YWT was produced by Oak Ridge National Laboratory (ORNL). PM2000 was produced by Plansee Inc., and MA956 and MA957 were produced by Special Metals Inc. (see Table 1). Every supplier used different production parameters resulting in slightly different grain structures. Due to nondisclosure policies of the material suppliers the exact production parameters like ball milling time, extrusion temperature, extrusion machines, powder source, amount of material produced in one heat, etc. are proprietary. PM2000, MA956, MA957, 12YWT and 14YWT specimens were exposed to flowing LBE in the DELTA Loop at LANL at a flow rate of 2 m/s at 535 °C for 200 h and 600 h after polishing them with 600 grit grinding paper. The oxygen content in the LBE was $\sim 10^{-6}$ wt%.

* Corresponding author. Address: Los Alamos National Laboratory, P.O. Box 1663, Los Alamos, NM 87545, USA.
E-mail address: peterh@lanl.gov (P. Hosemann).

0022-3115/$ - see front matter © 2007 Elsevier B.V. All rights reserved.
doi:10.1016/j.jnucmat.2007.05.049

Table 1
Nominal compositions and sources of the tested materials in wt%

Material	C	Cr	Al	Y_2O_3	W	Ti	Fe	Production
PM2000	.01	20	5.5	0.5	–	0.5	Balance	Extruded and rolled by Plansee
MA956	.04	20	4.5	0.5	–	0.4	Balance	Extruded and rolled by special metals
MA957	.01	14	–	.25	–	0.9	Balance	Extruded and rolled by special metals [11]
12YWT	0.2	12	–	.25	0.8	0.4	Balance	Extruded Kobe Steel, Ltd.
14YWT	0.2	14	–	.25	0.6	0.3	Balance	Extruded by Oak Ridge National Laboratory [10]

The sample size was 35 mm × 8 mm × 1 mm. The LBE flowed over the 35 mm × 8 mm area parallel to the 35 mm edge. After exposure to LBE, the specimens were analyzed using SEM/EDX in cross-section after a standard cutting, grinding and polishing (last step is 1 μm diamond polish) procedure. X-ray photoelectron spectroscopy (XPS) sputter depth profiling (SDP) was used for the MA956 and PM2000 specimens to determine the thickness and composition of the thin oxide layer. The samples analyzed in XPS had to be cleaned to remove residual LBE before these measurements. The sample cleaning was carried out using a hot ultrasonic (150 °C) glycerin bath for several minutes.

For the XPS SDP, a Surface Science Instruments SSX-100 fitted with a Nonsequitur Technologies Model 1401 ion gun for sputtering was used. The XPS binding energy analyses were referenced to the adventitious carbon 1 s line at 284.6 eV. The X-ray source for the XPS was a monochromatized and refocused aluminum Kα (1486 eV) source with a 0.1–1.0 mm diameter X-ray spot size. A sputter rate of 1.16 nm/s was used for SDP measurements. The O 2s, Cr 2p, Fe 2p, Y 3d and Al 2s peaks in the spectrum were used to analyze the elemental content in the oxide layer and the bulk material. After XPS measurements were completed, the sputter pits were analyzed using a JEOL JMS-5600 SEM instrument with an Oxford EDS detector. The acceleration voltage used was 15 keV. The same instrument was used to analyze the cross-section samples.

3. Results

Table 2 presents the thickness and a short description of the appearance of the oxide scale on each tested material measured by either SEM/EDX or XPS. The details of the corrosion behavior in LBE and the layer appearance are presented below for each material.

Table 2
Measured oxide layer thickness and layer appearance for the tested ODS samples

Material	Oxide layer thickness (μm)		Remarks
	200 h	600 h	
PM2000	–	0.2	Very thin protective oxide layer
MA956	–	1	Thin protective oxide layer
14YWT	10	15–18	Thick, compact, dense oxide layer
MA957	5–7	–	Strong localized grain boundary oxidation
12YWT	6–8	10–11	Thick, compact, dense oxide layer

3.1. PM2000

No corrosion or oxidation was observed in cross-section using SEM/EDX. Therefore XPS SDP measurements were performed to investigate the composition, thickness and state (oxidized or not oxidized) of each element in the near surface region. Fig. 1(a) and (b) shows two XPS SDP's in the surface (200 nm deep) and the near surface region (2 μm deep), respectively. Both SDPs were normalized using a final XPS survey spectrum after the SDP's were obtained. These SDP's show that the Fe content increases and the O content decreases with increasing depth into the substrate. Al content increased to 20–30 at.% to a depth of about 90 nm while deeper into the surface the Al content is only about 15 at.%. Y is enriched (1.7 at.%) to a depth of 50 nm. Further into the surface its content decreases to 0.18 at.%. Since the Y peak overlaps with the Bi peak it is possible that Bi is included as well. The Cr at the same time seems to be depleted (5–6 at.%) in the surface region (to about 100 nm deep) while the Cr content increases (to about 10 at.%) deeper into the surface.

3.2. MA956

This material did not show any oxide layer or corrosion attack in the SEM cross-section measurements after exposure to LBE at 535 °C for 600 h. Therefore an XPS analysis was performed. Fig. 2 presents the SDP performed on this material after exposure to LBE. These results show that the Fe content increases while the oxygen content decreases with increasing depth. But the oxygen content in the SDP does not decrease to the baseline. An oxygen content of 20 at.% was found as far as ~4.5 μm into the material. Due to the long sputter time, the max sputter depth was 4.5 μm. Y is slightly enriched in the near surface region, 0.12–0.1 at.% (to about 812 nm) compared to 0.04 at.% in the deeper region (2204 nm). Since the Y peaks overlaps the Bi peaks, the Y concentration could also include contribution from Bi remaining on the surface. Cr is slightly enriched in the near surface area from 14.4 at.% to 9 at.% in the deeper surface regions. In the near surface region an Al enrichment (~20.5 at.%) was found while in the deeper surface region the Al content decreased to 13.3 at.%.

3.3. 14YWT

The cross-sectional SEM measurements showed a thick multiple oxide layer after exposure to LBE. It is presented

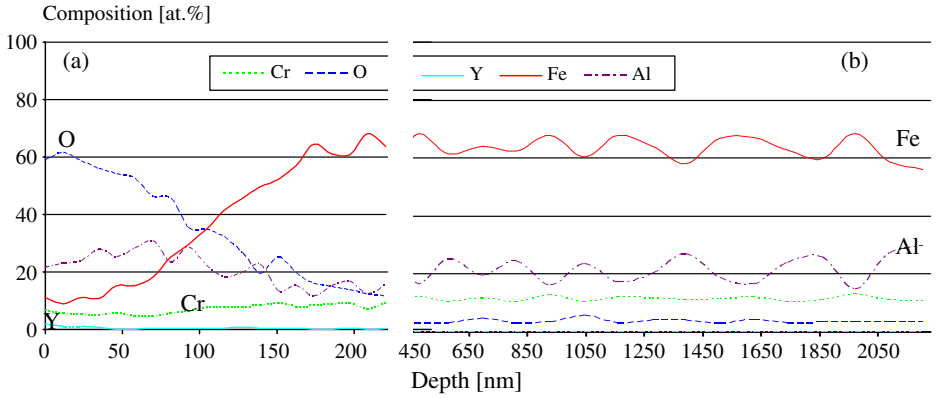

Fig. 1. (a) Shallow and (b) deep SDP of the material PM2000 using XPS. Bulk composition is 10 at.% Al, 19 at.% Cr, 0 at.% O, 0.5 at.% Y, balance Fe.

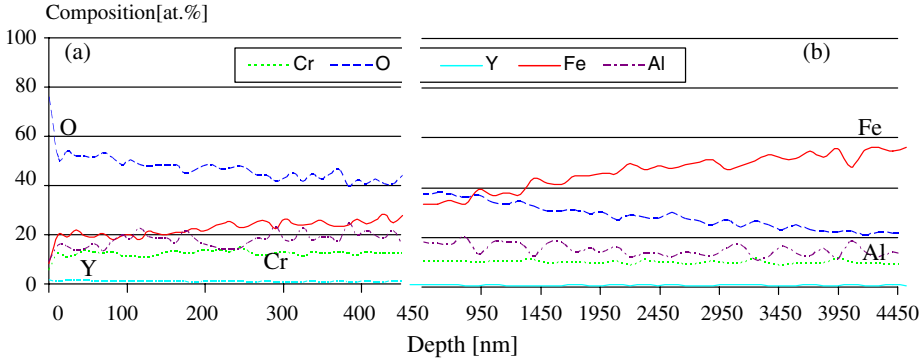

Fig. 2. (a) Shallow and (b) deep SDP of the material MA956. Bulk composition is 8 at.% Al, 19 at.% Cr, 0 at.% O, 0.5 at.% Y, balance Fe.

in Fig. 3 that the oxide layer thickness increased from about 10 μm (Fig. 3(a) 5 μm inner layer, 5 μm outer layer) after 200 h of exposure to about 15–18 μm (Fig. 3(b), 12 μm inner layer, 3–5 μm outer layer) after 600 h exposure to LBE. Fig. 3(c) presents the EDX line scan at the location marked in Fig. 3(b). It can be seen that the outer oxide layer is slightly Cr enriched and Fe depleted compared to the inner oxide layer. The composition in the thick inner layer is very homogeneous and does not change significantly. No cracks between the inner layer and the substrate were detected. Only a few cracks between the outer layer and the inner layer were detected after 600 h exposure to LBE.

3.4. MA957

TEM analysis performed by Hoelzer [13] (Fig. 9) prior to this study revealed an anisotropic grain structure. The grains appear to be elongated (2–5 μm long and 1–2 μm wide). The sample tested in the corrosion experiment showed a clear and dense double oxide layer structure after exposure in LBE for 200 h. Underneath the inner oxide layer some localized grain boundary oxidation (<0.5 μm deep) was detected (marked in Fig. 4(a)). The inner layer is about 3 μm thick while the outer layer is 5–7 μm thick. After 600 h exposure to LBE, very deep and strong localized oxidation was found (see Fig. 4(b)) underneath the inner oxide layer. The line scan across the dense oxide layer after 200 h exposure is shown in Fig. 4(c) at the marked area in Fig. 4(a). It can be seen that the oxygen content in the double oxide layer is very high especially in the border region between the inner and outer layer. The Fe is depleted and the Cr is slightly enriched throughout the entire oxide layer. The inner layer has a slightly higher Cr content while the Fe is depleted in this region.

3.5. 12YWT

The SEM cross-section measurements showed a 3 μm thick inner oxide layer and a 3–5 μm outside oxide layer after 200 h exposure to LBE. No selective oxidation or corrosion was detected. After 600 h exposure the inner oxide layer grew to a thickness of about 5 μm and the outer oxide layer to a thickness of about 5–6 μm. The EDX line scan of the 600 h exposed sample is given in Fig. 5(c). It can be seen that Cr is enriched in the oxide layers while Fe is depleted. The main difference between the outer and inner oxide layer is that the inner oxide has a slightly higher Cr content.

4. Discussion

4.1. PM2000

The SDP in Fig. 1 presents the elemental concentrations vs. sputter depth on the PM 2000 surface. XPS shows

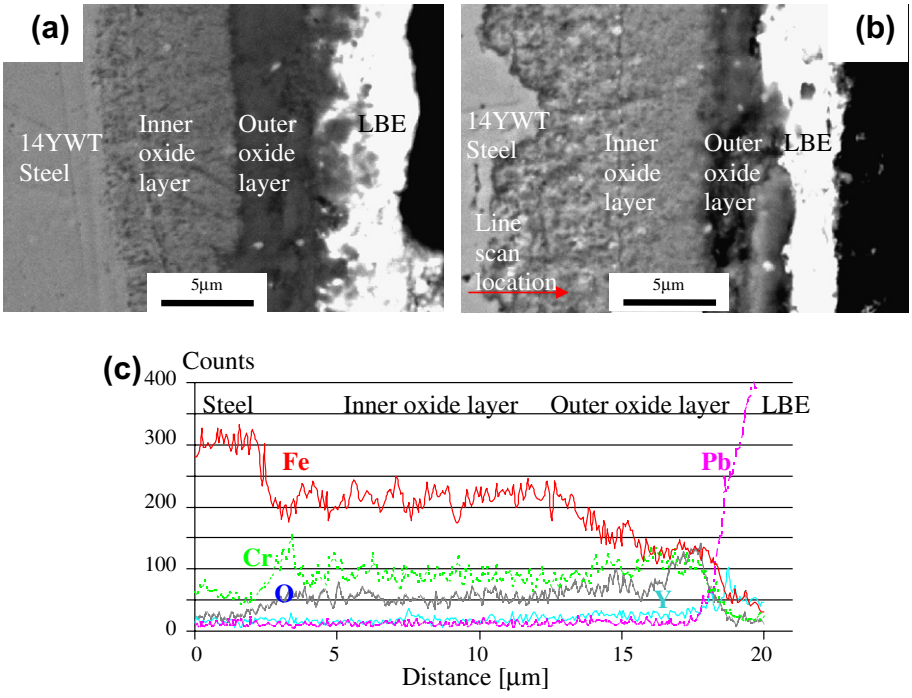

Fig. 3. (a) SEM image of 14YWT after 200 h exposure in LBE; (b) 600 h exposure sample; (c) EDX line scan showing the compositions of the oxide layer at the location marked in (b).

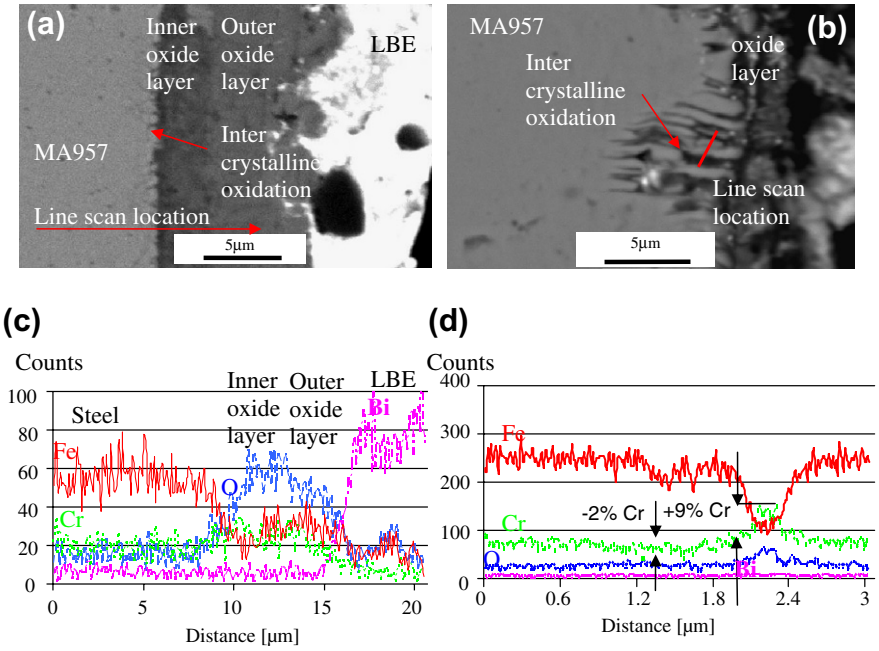

Fig. 4. (a) Oxide layer formed on MA957 after 200 h exposure to the LBE; (b) oxide structure after 600 h exposure; (c) EDX line scan taken at the marked area in image (a); (d) EDX line scan taken at the area marked in (b) with a red line. (For interpretation of the references in colour in this figure legend, the reader is referred to the web version of this article.)

which of the elemental species is oxidized and which is not. Table 3 compares the literature values for binding energy for each element found in the SDP, with those recorded as a function of depth. The NIST X-ray photoelectron spectroscopy database [5] was used for the literature data. Fe is oxidized to a total depth of 23 nm. The Cr is oxidized to a total depth of 58 nm. The analysis of Al is more difficult because the Al oxidized peak overlaps with the Al metal peak. Al is the second strongest oxide forming element (low Gibbs energy according to the Ellingham diagram) of the elements observed here. Therefore it is assumed that Al is oxidized as well. It was not possible

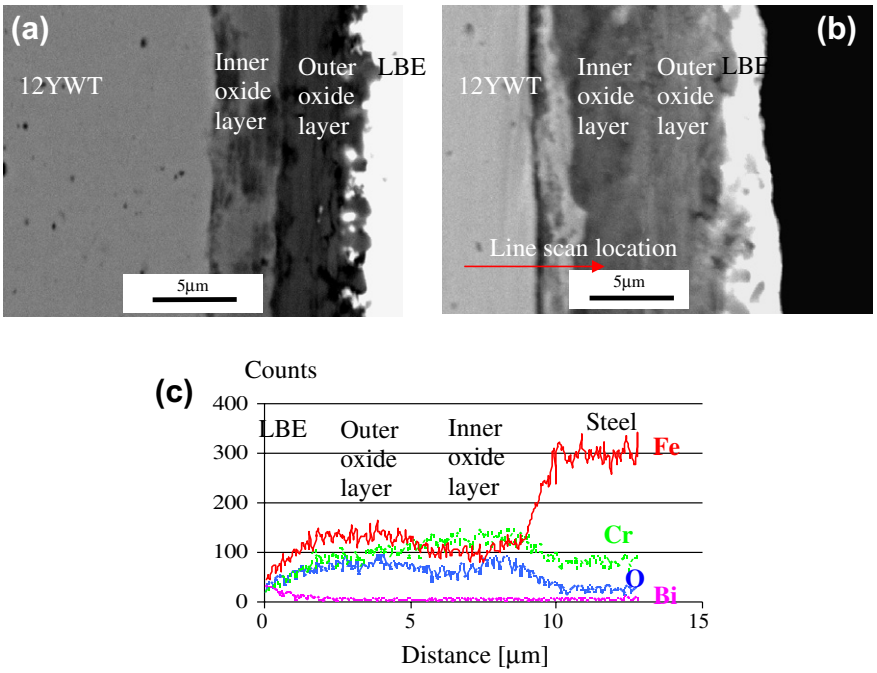

Fig. 5. (a) Oxide layer formed on 12YWT after 200 h exposure to LBE; (5) oxide layer after 600 h exposure to the LBE; (c) EDX line scan of the area marked in (b).

Table 3
Binding energies documented in the literature [5] and found in the XPS SDP at the material PM2000

Element	Binding energy of the data point in the SDP (depth in nm, binding energy in eV)									Binding energy (eV) from the literature [5]	
Depth (Å)	0	116	232	348	464	580	696	2204	Bulk	Oxidized	Metal
Fe 2p	711.2	710.14	710.3	707.1	707.4	707.2	707.4	707.7	707.8	709.0–711.4	706.8–707.5
Cr 2p	577.3	576.8	576.7	576.7	576.3	576.2	574.5	574.2	574.8	576.1–576.8	573.8–574.7
Al 2s	120.7	120.2	121.3	120.7	120.5	120.8	120.5	121.3	119.2	116.8–121.0	118.0–118.2
Y 3d3	156.8	157.4	157.4	158.0	157.3	157.2	157.0	157.5	160.3	157.4–160.7	158.05

to determine whether Y is oxidized in the near surface region or not because the binding energies of Y oxidized and Y metal are too close to each other. But Y is added to the material during ball milling in the form of Y_2O_3 powder. Therefore it is assumed that Y exists in the oxide form in the bulk material (Y_2O_3 has also the lowest Gibbs energy of the observed elements). The binding energy of Y 3d3 overlaps with the binding energy of Bi 4f7 (157 eV binding energy). Therefore Bi cannot be differentiated from Y. It was previously reported [6] that Al_2O_3 layers can act as diffusion barriers. The presence of Y also slows down the diffusion at grain boundaries [7]. Previously work shows [8] that nickel base alloys with an Al content above 5 wt% form a dense and protective oxide layer in oxidizing gaseous environment at elevated temperatures. The XPS results reported here show a similar behavior of the F/M material. It appears that under these test conditions Al forms a stable and protective Al_2O_3 layer (Gibbs energy is the second lowest of the observed elements according to the Ellingham diagram) which acts as a diffusion barrier for further oxidation. Pure α-Al_2O_3 layers act as very good diffusion barriers due to their hcp structure with very few defects [7]. This results in very low oxygen and metal diffusion coefficients [9] through Al_2O_3. Therefore only very little oxygen and metal ions can diffuse through this barrier. It also appears that the low amount of oxygen which still diffuses through that initial oxide barrier oxidizes the metals according to the Gibbs free energy of its oxides. At the surface all elements are oxidized, but deeper into the bulk only the more active elements are oxidized. Fig. 6 presents the measured amount of oxygen in the surface and the amount of oxygen which should be there if the marked elements are oxidized (Cr_2O_3, Fe_3O_4, Al_2O_3 and Y_2O_3). They show good agreement until a depth of 190 nm. At that point it seems that there is not enough oxygen to oxidize all of Al and Y. This comparison also allows the determination of the depth to which the Al and Y is oxidized, which is difficult to do using the XPS binding energies because of their spectral overlap.

Over all, PM 2000 seems to have the thinnest and most protective oxide layer of the tested materials.

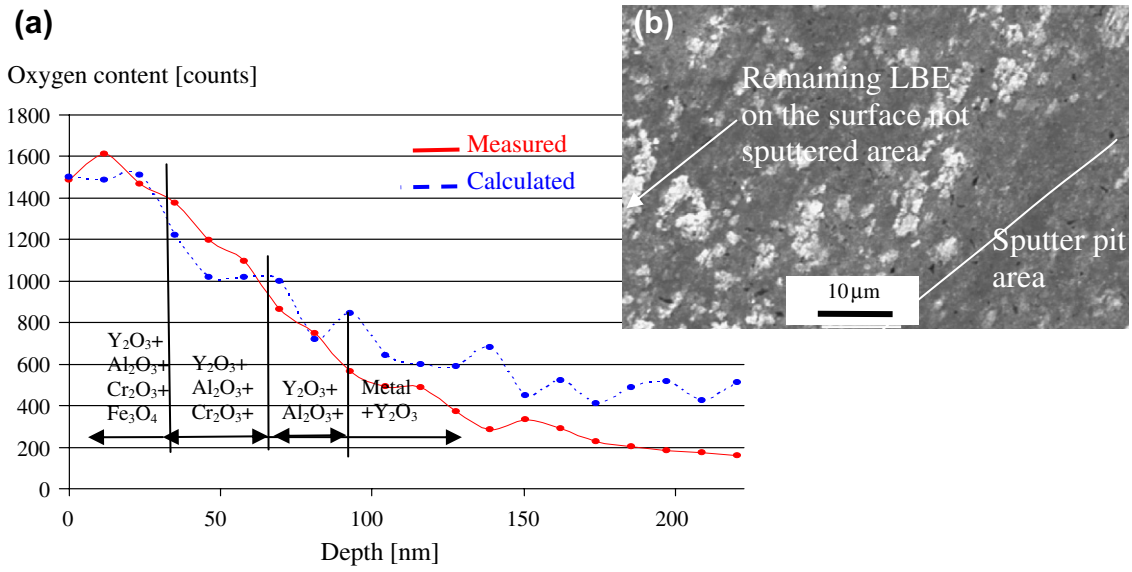

Fig. 6. (a) Comparison at PM2000 between the measured amount of O_2 in the oxide layer and the calculation based on the stoichiometric amount of O_2 in Cr_2O_3, Fe_3O_4, Al_2O_3 and Y_2O_3; (b) SEM image of the surface after exposing the sample to LBE.

4.2. MA956

An analysis of the oxidation state was done by measuring the XPS SDP's on this material. Table 4 shows that Fe is oxidized in the first 116 nm and Cr is oxidized in the first 1160 nm. Due to the overlap of the Al_2O_3 peak with the Al peak, it cannot be determined to which depth Al is oxidized with the XPS measurements. It is assumed that Al is oxidized if there is oxygen available for oxidation (Al has the second lowest Gibbs energy of the observed elements, Y has the lowest). Fig. 7(a) presents the measured oxygen curve and the calculated oxygen curve based on the assumption that the alloying elements are oxidized according to Table 3. The SEM image in Fig. 7(b) shows also that some areas don't show strong surface attack while some other areas show pitting. This leads to the assumption that a non uniform oxide layer was formed on the surface. Therefore in local areas, deeper oxidation or corrosion

Table 4
Binding energies documented in the literature [5] and found in the XPS SDP at the material MA956

Element	Binding energy of the data point in the SDP (depth in nm, binding energy in eV)							Binding energy in the literature	
Depth (Å)	0	104	116	580	696	4524	Bulk	Oxidized	Metal
Fe 2p	710.7	710.2	707.0	707.2	707.1	707.2	707.2	709.0–711.4	706.8–707.5
Cr 2p	577.9	577.4	574.4	576.7	574.9	574.3	574.5	576.1–576.8	573.8–574.7
Al 2s	120.7	120.4	120.0	119.3	120.6	120.9	117.8	116.8–121.0	118.0–118.2
Y 3d3	159.6	157.2	157.2	157.3	156.9	158.0	160.3	157.4–160.7	158.05

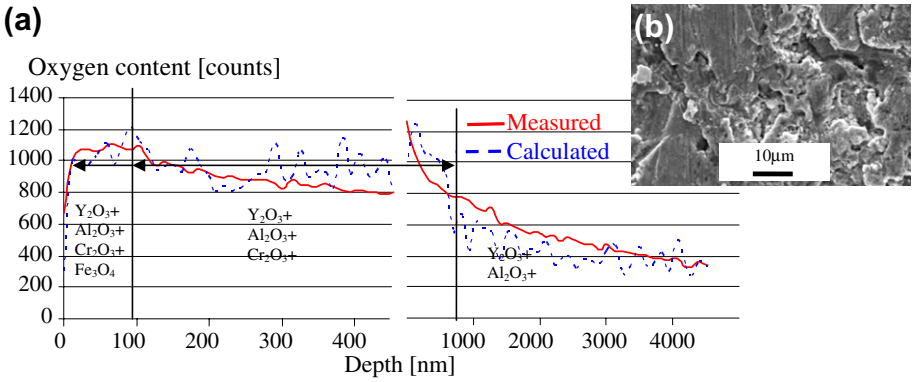

Fig. 7. (a) Comparison at MA956 between the measured amount of O_2 in the oxide layer and the calculation based on the stochiometric amount of O_2 in Cr_2O_3, Fe_3O_4, Al_2O_3 and Y_2O_3; (b) SEM image of the surface after exposing the sample to LBE.

occurred. Based on the fact that XPS SDP averages over the entire surface it can be understood that the spectrum shows a deeper overall surface oxidation. It can also explain why the calculated amount of oxygen (Fig. 7(a)) does not agree with the measurements as well as for PM2000. In Ni base superalloys, it is known [8] that a continuous dense protective oxide layer is only observed for Al content above 5 wt%. So it seems that at least 5 wt% Al is needed in these ferritic/martensitic steels in order to form a dense and protective oxide layer.

4.3.14YWT

This material showed homogeneous multiple oxide layers. No selective oxidation like pitting or grain boundary oxidation was found. The oxide layers are also very well bonded to the surface and to each other. No separation cracks were observed. As the material is exposed longer to LBE the outer oxide layer thickness seems to decrease slightly while the inner layer clearly grows thicker. This behavior can be understood using Li and Zhang's model [14]. There it is described that the alloying elements are in solution equilibrium between the outer layer and LBE. Therefore the most soluble element (in this case the Fe) will continuously be leached out of the oxide layer while the remaining pores are fast diffusion paths for the oxygen towards the inner oxide layer. The EDX cross-section profile reveals that inner oxide layer is Fe and Cr rich. The outer oxide layer is clearly Fe depleted after 600 h exposure to LBE. This also supports Li and Zhang's model. TEM measurements performed by Hoelzer [12] show that the grain size of this material is between 200 nm and 500 nm and the material does not have a very strong texture. It is assumed that the fine grain structure (compared to MA957) leads to faster and more homogeneous oxidation because of higher grain boundary density (see Fig. 8).

4.4. MA957

This material behaves very differently from 14YWT although their compositions are very similar. This material showed, especially after longer exposure (600 h), strong localized corrosion (localized inter crystalline oxidation) to a maximum depth of about 15 μm. A line scan across the intergranular corroded areas (see Fig. 4(b) and (d)) shows that a strong Cr enrichment in these areas took place while the area surrounding the Cr enriched oxidized grain boundary is slightly Cr depleted. As for all the tested materials, the total corrosion rate or oxidation depth can not be determined because it is not known how much material was removed from the surface. If an absolute corrosion rate needs to be measured the sample must be marked (using an inert coating on its surface) before exposing it to the LBE. The grains of MA957 are much larger (1–2 μm) than that of 14YWT (see Fig. 9). The localized oxidation correlates to the grain structure (see Fig. 9) and leads to the speculation that the grain boundaries act as fast diffusion paths inside the material. The depth of the oxidation in the grain boundaries of this material was not significantly greater than the homogeneous oxidation depth in 14YWT.

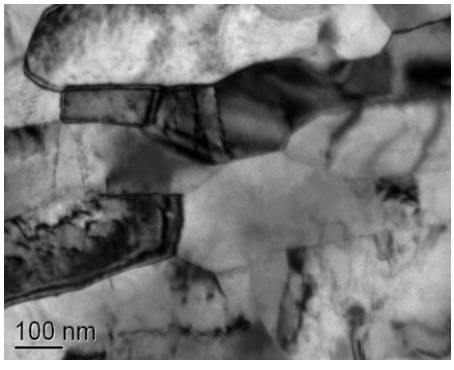

Fig. 8. TEM image from 14YWT made by Hoelzer [13]. The grain sizes are between 200 nm and 500 nm.

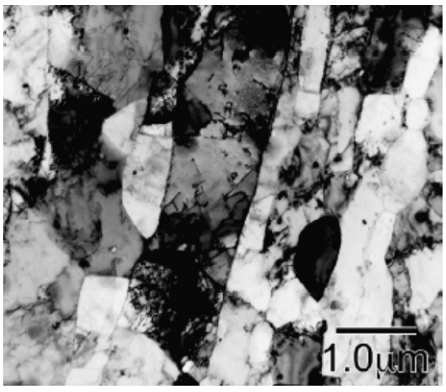

Fig. 9. TEM image from MA957 made by Hoelzer [12]. The grain sizes are between 1 and 2 μm and show a strong texture.

4.5. 12YWT

Homogeneous oxidation is observed in this material (Fig. 5). No cracking in the oxide layer was observed after 200 h exposure to the LBE. After 600 h exposure, some separation between the bulk and the oxide layer was observed. It is remarkable that the oxidation rate is very similar to the 14YWT although the Cr content is 2% points lower. This indicates that at these Cr levels, the additional Cr content does not have a large influence on the corrosion behavior above a certain Cr level threshold. Grain structure (comparing MA957 and 14YWT) appears to have a larger influence on the corrosion mechanism than the 2% difference in Cr content.

5. Conclusion

- PM 2000 shows a very dense, thin and protective oxide layer in LBE at 535 °C after up to 600 h testing due to its higher Al content.
- It is found that the compositions of the oxide layers found on the Al alloyed materials change with depth.

Elements are oxidized based on the amount of oxygen available for oxidation and the free energy of the oxide.

- So far PM2000 shows the thinnest oxide layer without selective oxidation and therefore has the most promising capability to withstand LBE corrosion at high temperatures.
- It appears that at least 5.5 wt% Al in the alloy is necessary in order to form a protective Al enriched oxide.
- MA956 is similar to PM2000 but the oxide layer formed appears thicker, has a higher growth rate and some localized oxidation. Therefore it is considered to be less corrosion resistant than PM2000.
- 14YWT shows a very homogeneous thick oxide layer but it is significantly thicker than the oxide layer found on PM2000.
- MA957 shows deep localized grain boundary oxidation. The grain boundary oxide is strongly Cr enriched while the surrounding area is slightly Cr depleted.
- 14YWT and MA957 have very similar nominal compositions. But the corrosion behaviors of both materials are very different. This may be due to the different grain structure caused by different production parameters.
- 12YWT has a 2% point's lower Cr content than 14YWT but the appearances of the oxide layer and structure are very similar. The oxide growth for both 12YWT and 14YWT were relatively thick and could lead to a significant loss of material in long term operations.

Acknowledgements

The authors wish to thank Professor Dr Gregor Mori (University of Leoben, Austria) for his academic support, Dr David Hoelzer (ORNL, TN, USA) for providing the 14YWT, 12YWT and MA957 TEM results, Jenny Welch and Dan Koury (UNLV, NV, USA) for their supporting work on the SEM, and Mike Madrid (LANL, NM, USA) for his support operating the DELTA loop.

References

[1] C. Rubbia, J.A. Rubio, S. Buono, F. Carminati, Conceptual design of a fast neutron operated high power energy amplifier, CERN/AT/95-44 (ET), 29 September 1995.
[2] M. Turker, T.A. Hughes, Oxid. Metals 44 (1995) 235.
[3] R.A. Versaci, D. Clemens, W.J. Quadakkers, R. Hussey, Solid State Ionics 59 (1993) 235.
[4] P. Pérez, Corros. Sci. 44 (2002) 1793.
[5] C.D. Wagner, A.V. Naumkin, A. Kraut-Vass, J.W. Allison, C.J. Powell, John R. Rumble, Jr., NIST XPS database, http://srdata.nist.gov/xps/.
[6] J. Mueller, D. Neuschütz, Vacuum 71 (2003) 247.
[7] M. Legall, A.M. Huntz, B. Lesage, C. Monty, J. Bernardini, J. Mater. Sci. 30 (1995) 201.
[8] E. Kunze, Corrosion and Corrosion Protection, 2001, ISBN: 3-527-29994-7 (in German).
[9] D.W. Kingery, H.K. Bowen, D.R. Uhlmann, Introduction to Ceramics, Wiley, 1960, ISBN 0-471-47860-1.
[10] M.J. Alinger, G.R. Odette, D.T. Hoelzer, J. Nucl. Mater. 329–333 (2004) 382.
[11] M.K. Miller, D.T. Hoelzer 1, E.A. Kenik 2, K.F. Russell, J. Nucl. Mater. 329–333 (2004) 338.
[12] M.K. Miller, D.T. Hoelzer, E.A. Kenik, K.F. Russell, in: Presentation at the International Conference of Fusion Reactor Materials 11 (ICFRM 11), Kyoto, Japan, 2003.
[13] D.T. Hoelzer, J. Bentley, M. Sokolov, M.K. Miller, G.R. Odette, M.J. Alinger, J. Nucl. Mater. 367–370PA (2007) 166.
[14] J. Zhang, N. Li, Y. Chen, J. Nucl. Mater. 1 (2005) 342.